International Journal of Solids and Structures 46 (2009) 1793–1804

Contents lists available at ScienceDirect

International Journal of Solids and Structures

journal homepage: www.elsevier.com/locate/ijsolstr

A representative volume element based on translational symmetries for FE analysis of cracked laminates with two arrays of cracks

S. Li [1], C.V. Singh, R. Talreja *

Department of Aerospace Engineering, Texas A&M University, 710 H.R. Bright Building, College Station, TX 77843-3141, USA

ARTICLE INFO

Article history:
Received 20 August 2008
Received in revised form 9 January 2009
Available online 21 January 2009

Keywords:
Representative volume element (RVE)
Unit cell
Cracked laminate analysis
Symmetry
Boundary conditions

ABSTRACT

A methodology is proposed for the construction of a representative volume element (RVE) for analysis of laminated composites containing two arrays of ply cracks running in different directions. The only requirement is that the cracks in any ply are uniformly spaced, and if more than one ply of a given orientation is cracked, then the crack spacing of individual plies must only be in exact multiples of each other. The spacing of cracks in the two directions can be fully independent. The RVE is constructed through a systematic consideration of translational symmetries present in the cracked laminate. As a result, the boundary conditions on the RVE can be imposed without compromising accuracy. Examples of the application of the RVE methodology are given to illustrate its broad capability and a finite element (FE) stress analysis is performed for these cases to illustrate results such as the crack surface displacements, local stress fields and RVE-averaged elastic properties. For one case, the average properties are compared with experimental results, showing good agreement.

Published by Elsevier Ltd.

1. Introduction

Fiber-reinforced composite laminates develop cracks in the plies when loaded mechanically and/or thermally. These cracks lie along the fibers in the plies, and are referred to as ply cracks, matrix cracks, or transverse cracks because of their planes being normal to the ply mid-plane. In practical structures the laminates have plies of multiple orientations and therefore under a general loading they can develop ply cracks of multiple orientations. The ply cracks of an individual orientation form an array of parallel cracks, whose spacing is generally irregular initially, but tends to become uniform, increasingly as the cracks come closer. In the presence of these cracks, a laminate responds differently than in its pristine state and although failure is seldom caused by these cracks directly, they can lead to delamination and eventual laminate failure. For structural integrity and durability assessment it is necessary to perform deformational and failure analysis of laminates with ply cracks.

The early analytical approaches to laminates with cracks relied on the shear lag concept and were applied to cross-ply laminates with cracks in the transverse plies (Garrett and Bailey, 1977). Although numerous extensions of the shear lag analysis exist for cracks of multiple orientations, the accuracy of such analyses cannot generally be assessed. More accurate analysis is given by the variational method, which was first published in the English literature by Hashin (1985) for cross-ply laminates with cracks in transverse plies and later extended to these laminates with two orthogonal crack arrays (Hashin, 1987). Although the variational analysis can be made more accurate, as in Varna and Berglund (1991), it cannot be extended to non-orthogonal cracks. Other analyses, such as the finite strip analysis by Li et al. (1994) and stress transfer by McCartney (1992) are also limited to cases involving aligned cracks. More recently, stiffness prediction for off-axis laminates with ply cracks in two symmetrically placed off-axis plies has been attempted (Singh and Talreja, 2008) using the so-called 'synergistic damage mechanics'. This approach requires knowledge of crack opening displacement which should be obtained numerically. The current work will be useful in that context.

It cannot be denied that a numerical analysis, such as the finite element (FE) analysis, is inevitable for general cases of laminates with non-uniformly distributed ply cracks in multiple, non-orthogonal orientations. At the same time, an FE analysis can become invalid and impractical if care is not exercised to reflect the model geometry, e.g. by making use of symmetry appropriately. An important step in the process of conducting FE analysis for cracked laminates is to set up an appropriate representative volume element (RVE). An important requirement for such RVE is that it has representation of all material properties (e.g. elastic moduli) and geometry (orientation, sequence and thickness of plies), as well as a minimum representative number of cracks that contribute to the subject of interest. In a simple case of a cross-ply laminate with

* Corresponding author. Tel.: +1 979 458 3256; fax: +1 979 845 6051.
E-mail address: talreja@aero.tamu.edu (R. Talreja).
[1] On leave from School of MACE, University of Manchester, Manchester M60 1QD, UK.

0020-7683/$ - see front matter Published by Elsevier Ltd.
doi:10.1016/j.ijsolstr.2009.01.009

uniformly distributed transverse ply cracks, loaded by uniform axial traction, the RVE is simply a unit cell of rectangular shape, extending from one crack to the next in the axial direction and having laminate thickness as its lateral dimension. Due to two orthogonal planes in the unit cell only a quarter-cell region suffices for FE analysis. At the other end, RVE for a general laminate with cracks in multiple orientations will inevitably be a three-dimensional volume containing a multitude of cracks. Without some degree of justifiable simplification an FE analysis of the most general RVE can become impractical and difficult to interpret.

The present effort is devoted to proving simple rules for constructing an RVE for the case of a laminate that contains ply cracks in two orientations, not necessarily orthogonal. The crack spacing in the arrays of the two orientations can be independent of each other. The only requirement is that in each of these orientations, cracks must be spaced either at a constant distance or at distances that are exact multiples of one another. The cracks of a given orientation can also be spread over plies of that orientation. The proposed construction invokes invariance with respect to translation of a basic unit consisting of a rectangular region defined by the two orientations. The approach adopted here stems from the development of unit cells establish for micromechanical analysis of unidirectionally fiber-reinforced or particle-reinforce composites (Li, 1999, 2001; Li and Wongsto, 2004). The RVE construction is developed for different cases to illustrate the breadth of its applicability. FE analysis is performed for each case and its results are discussed and for one case the results are compared with experimental data on elastic moduli. Several related studies can also be found in the literature. For instance, Noh and Whitcomb (2001) used periodic boundary conditions in evaluation of effective properties of cracked laminates but the layup of the laminates and the placement of cracks in the laminates are rather restrictive. Xia et al. (2003) developed RVE for evaluation of effective properties in angle ply (i.e. $\pm\theta$) laminates. Other work relevant to analysis of periodic microstructures in composites include studies by Xia et al. (2006), Grufman and Ellyin (2007) and Jin et al. (2008).

2. Macroscopic strains and corresponding displacement field

When a laminate is subjected to a macroscopically uniform strain field, ε_x^0, ε_y^0 and γ_{xy}^0, under in-plane loading, the relative displacements between two points P and P' can be expressed as (Li and Wongsto, 2004)

$$\begin{aligned} u' - u &= (x' - x)\varepsilon_x^0 + (y' - y)\gamma_{xy}^0 \\ v' - v &= (y' - y)\varepsilon_y^0 \\ w' - w &= 0 \end{aligned} \tag{1}$$

where u, v and w are the displacements at point P while u', v' and w' are those at P'. It can be pointed out that the expression of the above displacement field is not unique and a different expression would, however, only differ from the above by a rigid body rotation.

The above relative displacements will be essential for establishing the boundary conditions for the RVE to be used for the FE analysis of such cracked laminates as will be presented below.

3. Geometric considerations

Assume a laminate of arbitrary layup in which there are two arrays of ply cracks running at angles θ_1 and θ_2, measured with respect to the reference axis x of the laminate coordinate axes (x,y,z), as sketched in Fig. 1(a). Since the cracks are aligned with the fiber direction in the ply, these angles also represent the fiber directions in the cracked plies. Let there be as many such cracked plies as practically possible in the laminate (for illustration in Fig. 1(a), only one cracked ply in each of the two orientations is shown) and let them be placed in an arbitrary sequence. However, in every cracked ply of either array, the crack spacing must be the same, or if different, then it must be in exact multiples of one another. The crack spacing in the two directions could, however, be independent of each other. It is also assumed that the in-plane dimensions of the laminate are sufficiently larger than those of the RVE and hence the RVE is free from the effects due to the free edges of the laminate.

In the mid-plane of the laminate, a tessellation is introduced using a grid system of which each family of gridlines is parallel to an array of cracks, as sketched in Fig. 1(b). The gridlines in each family are spaced at the crack spacing of the corresponding array. When the plane of the laminate is partitioned with the grid system, all the patches created are identical. Any of these can be chosen as the master cell and the rest can be reproduced by translational transformation as an image of this cell. The mapping from the origin to its image can be characterized by two independent transformations in the (ξ,η) coordinate system, aligned with the crack directions (Fig. 1(b)): translations by m spaces along the ξ-axis and n spaces along the η-axis. Taking an arbitrary point P in the master cell as the origin, the corresponding point P' in the image cell is then given by the transformation represented by m and n. In the case of Fig. 1, $m = 2$ and $n = 1$.

In accordance with the mapping, $P(x,y,z) \to P'(x',y',z')$, the coordinates of points P and P' are related as follows:

$$\begin{aligned} x' &= x + ml_1\cos\theta_1 + nl_2\cos\theta_2 \\ y' &= y + ml_1\sin\theta_1 + nl_2\sin\theta_2 \\ z' &= z \end{aligned} \tag{2}$$

where

$$l_1 = b_2/\sin(\theta_2 - \theta_1) \quad \text{and} \quad l_2 = b_1/\sin(\theta_2 - \theta_1), \tag{3}$$

with b_1 and b_2 being the crack spacing in the two arrays and l_1 and l_2 the side lengths of the repeated cell as indicated in Fig. 1(b).

4. RVE and its boundary conditions

The geometric symmetries in the sense of translations allow the use of the master cell as an ideal "basic cell". However, in order to develop an RVE from this cell, a set of appropriate boundary conditions have to be placed to account for all the necessary geometry, displacement and traction continuity conditions between this cell and all other cells surrounding it. The translational transformations in the mapping process already account for the continuity of geometry, as described in the previous section. The displacement continuity based on the same translational transformations is described next.

Consider the master cell as shown shaded in Fig. 1 with sides A, B, C and D. The cell to its right is its image given by the transformation $m = 1$, $n = 0$. The right side A of the master cell is also the left side of this image cell, which by the transformation is the image of the left side B of the master cell. Thus the continuity conditions between the two cells will be fulfilled by the relationship between side A and side B of the master cell as imposed by the translational symmetry transformation.

Using $m = 1$ and $n = 0$ into the coordinates transformation (2), gives

$$\begin{aligned} x' - x &= l_1\cos\theta_1 \\ y' - y &= l_1\sin\theta_1 \\ z' - z &= 0 \end{aligned} \tag{4}$$

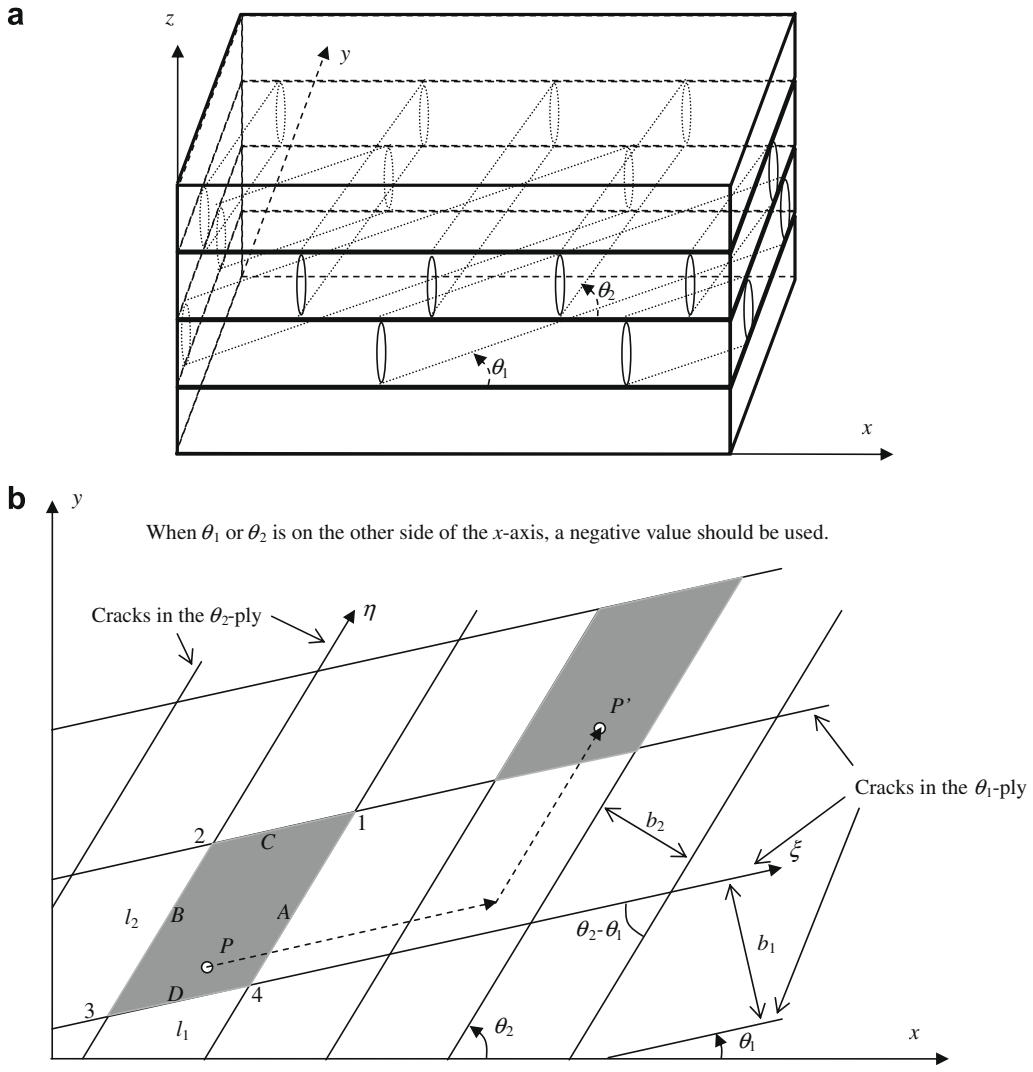

Fig. 1. (a) A 3D view of a cracked laminate. (b) A planner view of a cracked laminate with cells tessellated by the grid system.

Substituting the above into (1), the relative displacements between corresponding nodes on the two opposite sides A and B of the master cell are obtained as

$$\begin{aligned} &-u|_B + u|_A - l_1(\varepsilon_x^0 \cos\theta_1 + \gamma_{xy}^0 \sin\theta_1) = 0 \\ &-v|_B + v|_A - l_1 \varepsilon_y^0 \sin\theta_1 = 0 \\ &-w|_B + w|_A = 0 \end{aligned} \tag{5}$$

It is noted that these conditions represent continuity on the common surface between the master cell and the cell on its right, and therefore apply only to the continuous part of the side. If a crack lies along this side, these conditions would not apply on the part that has the crack surfaces because of the displacement discontinuity. Thus, in implementing these conditions digitally in a FE model, the nodes on the interfaces should be considered as part of the uncracked surface while they are excluded from the crack surface. If equation constraints as given in Eq. (5) are used to eliminate some degrees of freedom when implemented practically through an FE code, e.g. ABAQUS®, it is crucial for the user to be clear which ones are to be eliminated. For the sake of presentation in this paper, and also as a systematic guideline for potential users, the first term in each of Eq. (5) is eliminated. This is consistent with ABAQUS® applications and also the reason why these equations are presented in this particular manner. These considerations apply to all development hereafter.

Between sides C and D, relative displacements between corresponding nodes for the uncracked part of the interface are obtained in a similar manner. The transformation is represented by $m = 0$ and $n = 1$ in this case and hence,

$$\begin{aligned} &x' - x = l_2 \cos\theta_2 \\ &y' - y = l_2 \sin\theta_2 \\ &z' - z = 0 \end{aligned} \tag{6}$$

and

$$\begin{aligned} &-u|_D + u|_C - l_2(\varepsilon_x^0 \cos\theta_2 + \gamma_{xy}^0 \sin\theta_2) = 0 \\ &-v|_D + v|_C - \varepsilon_y^0 l_2 \sin\theta_2 = 0 \\ &-w|_D + w|_C = 0 \end{aligned} \tag{7}$$

Eqs. (5) and (7) together define the displacement boundary conditions for the RVE. When these conditions are imposed on the faces B and D, the degrees of freedom there are eliminated. Depending on the FE code used for the analysis, complications can sometimes arise. Firstly, these conditions have to be imposed in the forms of equations between unknown degrees of freedom of the RVE. Secondly, their imposition also introduces extra degrees of freedom,

ε_x^0, ε_y^0 and γ_{yz}^0, into the analysis and the code selected should have a mechanism to allow this. Both of the above can be accomplished with facilities such as 'equation constraints' or 'multiple point constraints (MPC)', which are available in many commercial FE codes, for instance, ABAQUS®. A third complication requires a bit further treatment as follows.

For the continuous part of the edges (viewed as corners in 2D), i.e. the intersections between the sides of the RVE, some of the conditions obtained for the nodes along it are duplicating. Among the four corners, 1, 2, 3 and 4, as shown in Fig. 1, both corners 2 and 4 are tied to corner 1 as well as to corner 3. In other words, a relationship between corners 3 and 1 can be established through corner 4, and another such relationship can be established through corner 2. These two relationships thus are duplicate of each other. This makes some of the equations from (5) and (7) redundant when they are imposed at corners. While redundant equations do not make any difference mathematically, they can cause errors in some of the FE codes, such as ABAQUS®, as each of such equation constraints will be used to eliminate one degree of freedom. When a redundant equation constraint arises, the code looks for a degree of freedom that has been eliminated already. This will be perceived as an error. It is therefore the user's responsibility to eliminate such redundant equations before these equation constraints are imposed. The way those corners are related provides the way of eliminating these redundant equations.

To implement this consideration, when faces for the sides are defined, the nodes long the edges (intersection of sides) at the corners are excluded. These edges at the corners are treated separately as follows. For the continuous part of an edge at a corner, say corner 1, including the node where cracks in the neighboring plies in different directions meet, the nodes on it are related to those at corners 2 and 4 according to (5) and (7), i.e.

$$\begin{aligned} &-u_2+u_1-l_1\left(\varepsilon_x^0\cos\theta_1+\gamma_{xy}^0\sin\theta_1\right)=0\\ &-v_2+v_1-\varepsilon_y^0 l_1\sin\theta_1=0 \qquad \text{for corner 2}\\ &-w_2+w_1=0 \end{aligned} \tag{8}$$

and

$$\begin{aligned} &-u_4+u_1-l_2(\varepsilon_x^0\cos\theta_2+\gamma_{xy}^0\sin\theta_2)=0\\ &-v_4+v_1-\varepsilon_y^0 l_2\sin\theta_2=0 \qquad \text{for corner 4}\\ &-w_4+w_1=0 \end{aligned} \tag{9}$$

The relationships between corner 3 and corner 1 established through corner 2 duplicates those established through corner 4 and hence one set, given below, suffices.

$$\begin{aligned} &-u_3+u_1-(l_1\cos\theta_1+l_2\cos\theta_2)\varepsilon_x^0-(l_1\sin\theta_1+l_2\sin\theta_2)\gamma_{xy}^0=0\\ &-v_3+v_1-(l_1\sin\theta_1+l_2\sin\theta_2)\varepsilon_y^0=0 \quad \text{for corner 3}\\ &-w_3+w_1=0 \end{aligned} \tag{10}$$

Eqs. (8)–(10) apply to the uncracked parts of the edges. In this way, all the independent equation constraints have been incorporated while redundant equation constraints have been left out. As they are imposed, the degrees of freedom on the edges at corners 2, 3 and 4 are eliminated. Since they represent continuity conditions, they are, of course, only imposed on the continuous parts of the edges at the corners, as stated above.

For the part of the edges within a crack surface, say for that running in the θ_1 direction, the discontinuity is present along a direction across the θ_1 direction, while continuity remains along the θ_1 direction. Thus, the following applies to this part of the edge, if the crack surface containing it is along the θ_1 direction

$$\begin{aligned} &-u_2+u_1-l_1(\varepsilon_x^0\cos\theta_1+\gamma_{xy}^0\sin\theta_1)=0\\ &-v_2+v_1-\varepsilon_y^0 l_1\sin\theta_1=0 \qquad \text{between corners 2 and 1}\\ &-w_2+w_1=0 \end{aligned} \tag{11}$$

and

$$\begin{aligned} &-u_3+u_4-l_1(\varepsilon_x^0\cos\theta_1+\gamma_{xy}^0\sin\theta_1)=0\\ &-v_3+v_4-\varepsilon_y^0 l_1\sin\theta_1=0 \qquad \text{between corners 3 and 4}\\ &-w_3+w_4=0 \end{aligned} \tag{12}$$

For the part of the edges at the corners within the crack surface running in the θ_2 direction, continuity remains intact along that direction. Thus, the following applies for this case:

$$\begin{aligned} &-u_4+u_1-l_2(\varepsilon_x^0\cos\theta_2+\gamma_{xy}^0\sin\theta_2)=0\\ &-v_4+v_1-\varepsilon_y^0 l_2\sin\theta_2=0 \qquad \text{between corners 4 and 1}\\ &-w_4+w_1=0 \end{aligned} \tag{13}$$

and

$$\begin{aligned} &-u_3+u_2-l_2(\varepsilon_x^0\cos\theta_2+\gamma_{xy}^0\sin\theta_2)=0\\ &-v_3+v_2-\varepsilon_y^0 l_2\sin\theta_2=0 \qquad \text{between corners 3 and 2}\\ &-w_3+w_2=0 \end{aligned} \tag{14}$$

This completes all the displacement boundary conditions introduced by the translational symmetry considerations. For their easy application, a sketch is presented in Fig. 2(a) to illustrate where each of the particular equation constraints should be imposed. Eqs (8), (11) and (14) have not been shown in Fig. 2, as they follow from Eqs. (10), (12) and (13), respectively. Eqs. (11)–(14) are required only if there are exposed crack surfaces on the sides of the RVE.

In terms of imposition of boundary conditions in a practical analysis, it might be advantageous to avoid exposing crack surfaces on the sides of the RVE. This can be easily achieved by offsetting the grid system in the ξ and η directions by an arbitrary amount, as shown in Fig. 2(b). This will not upset the translational symmetries in any way. By doing this, the boundary conditions will be easier to impose. However, the RVE will contain internal cracks, which makes the meshing more demanding, as a set of independent nodes will have to assigned to each side of the opposite surfaces of a crack. Between the options as sketched in Fig. 2(a) and (b), it will be entirely the users' choice, i.e. either easier meshing or easier boundary conditions.

The displacement boundary conditions on the RVE obtained above are necessary to facilitate an FE analysis without using any incorrect representation of the RVE. One should bear in mind that this RVE as constrained so far still allows rigid body translations in three directions. They need to be constrained as follows before an FE analysis can go ahead.

$$\begin{aligned} &u=0\\ &v=0 \quad \text{at any but only one free node}\\ &\qquad (\text{i.e. not subject to other constraints})\\ &w=0 \end{aligned}$$

The free node can be from corner 1 but not from other corners as the nodes there have already been constrained through Eqs. (8)–(14). The third constraint in Eq. (15) above should not be imposed if symmetry about the z-plane is assumed, e.g. when only half of the laminate thickness is analyzed for a laminate of symmetric layup.

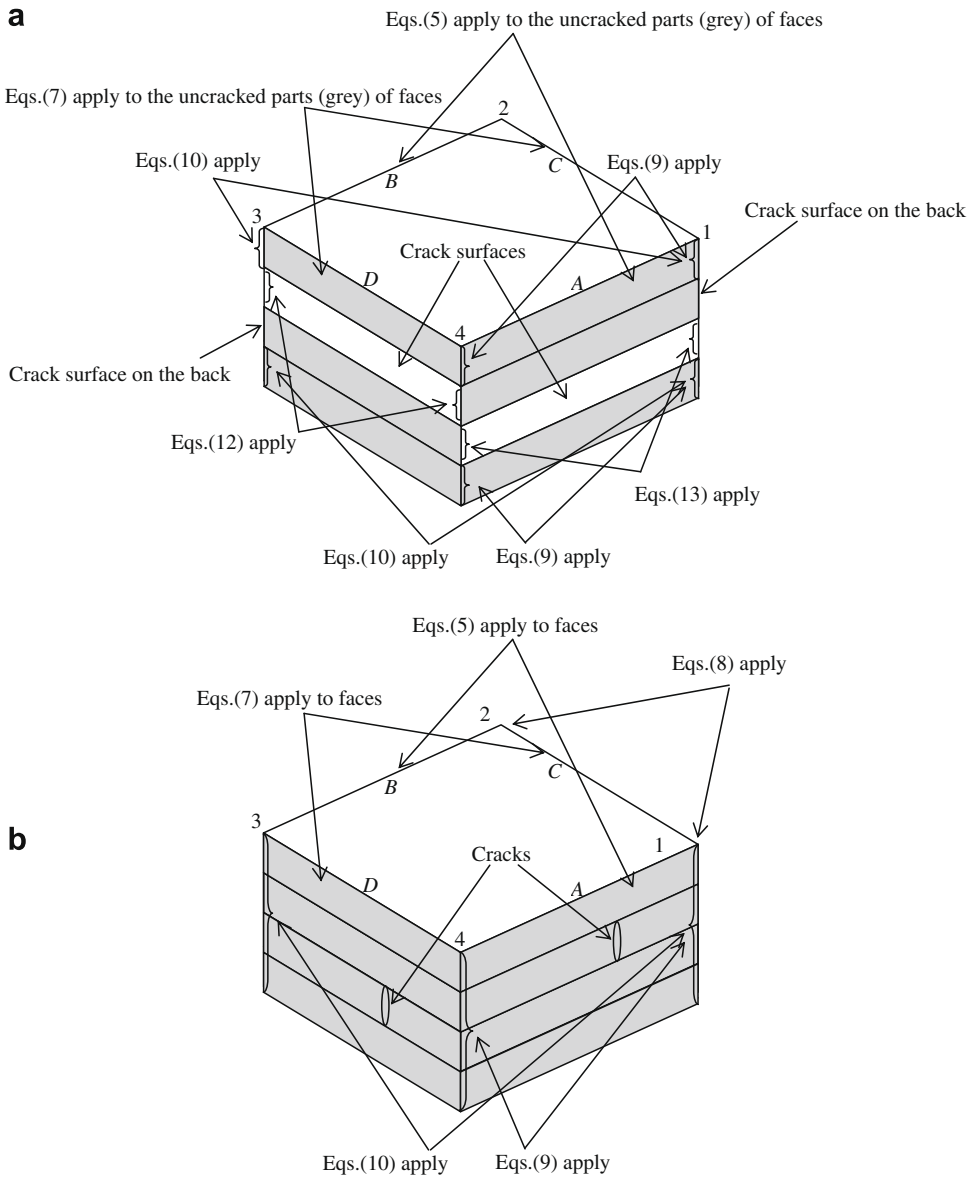

Fig. 2. (a) Illustration of the boundary conditions on the RVE with surface cracks. (b) Illustration of the boundary conditions on the RVE without surface cracks.

The rigid body rotations, however, have been constrained already by the symmetry transformations and no extra care has to be exercised in this respect by the user.

5. Traction boundary conditions

The continuity should also impose some relationships between the tractions on opposite sides of the RVE over the continuous part of the surfaces. They can be given as follows.

Given the periodic appearance of the RVE, the boundary $\partial\Omega$ can be split into two parts, $\partial\Omega^+$ and $\partial\Omega^-$, with outward normals on them denoted as n_i^+ and n_i^-, respectively, where $\partial\Omega^+$ and $\partial\Omega^-$ can be related through translational transformations (in a piecewise manner, as appropriate). Between the corresponding points on $\partial\Omega^+$ and $\partial\Omega^-$ the translations symmetry conditions require

$$\sigma_{ij}^+ n_j^+ + \sigma_{ij}^- n_j^- = 0 \tag{16}$$

where σ_{ij}^+ and σ_{ij}^- are the stresses on $\partial\Omega^+$ and $\partial\Omega^-$, respectively. These are the natural boundary conditions for the boundary value problem. Satisfaction of these conditions is achieved as a part of variational process as the total potential energy functional is minimized.

However, if the FE code is displacement based, as most existing commercial FE codes are, traction boundary conditions are natural boundary conditions, in the terminology of the variational principles. They should not be imposed since the variation (minimization in the case of linear elastic problem) of the total potential energy will imply them, as discussed in Li (2008). As far as a user is con-

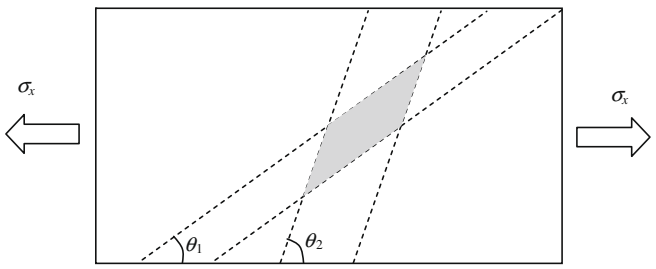

Fig. 3. Laminates to be analyzed in the Examples 6.1 and 6.3.

cerned, the traction boundary conditions (16) can be ignored in order to apply the RVE presented here.

6. Examples of applications

To illustration the application of the RVE established above, two examples have been chosen. Given the fact that existing results are scarce in the literature, direct comparisons with available results are not to be pursued. However, the results obtained will be discussed in order to justify them as far as possible. The plies in all the cases considered here are assumed to be standard graphite-epoxy with a ply thickness of 0.25 mm and with the following elastic properties:

$$E_1 = 44.7\,\text{GPa};\quad E_2 = 12.7\,\text{GPa};\quad G_{12} = 5.8\,\text{GPa}\quad \text{and}\quad \nu_{12} = 0.297$$

where E_1 and E_2 are the Young's moduli in the fiber and transverse directions, respectively, G_{12} is the in-plane shear modulus and ν_{12} is the axial Poisson's ratio.

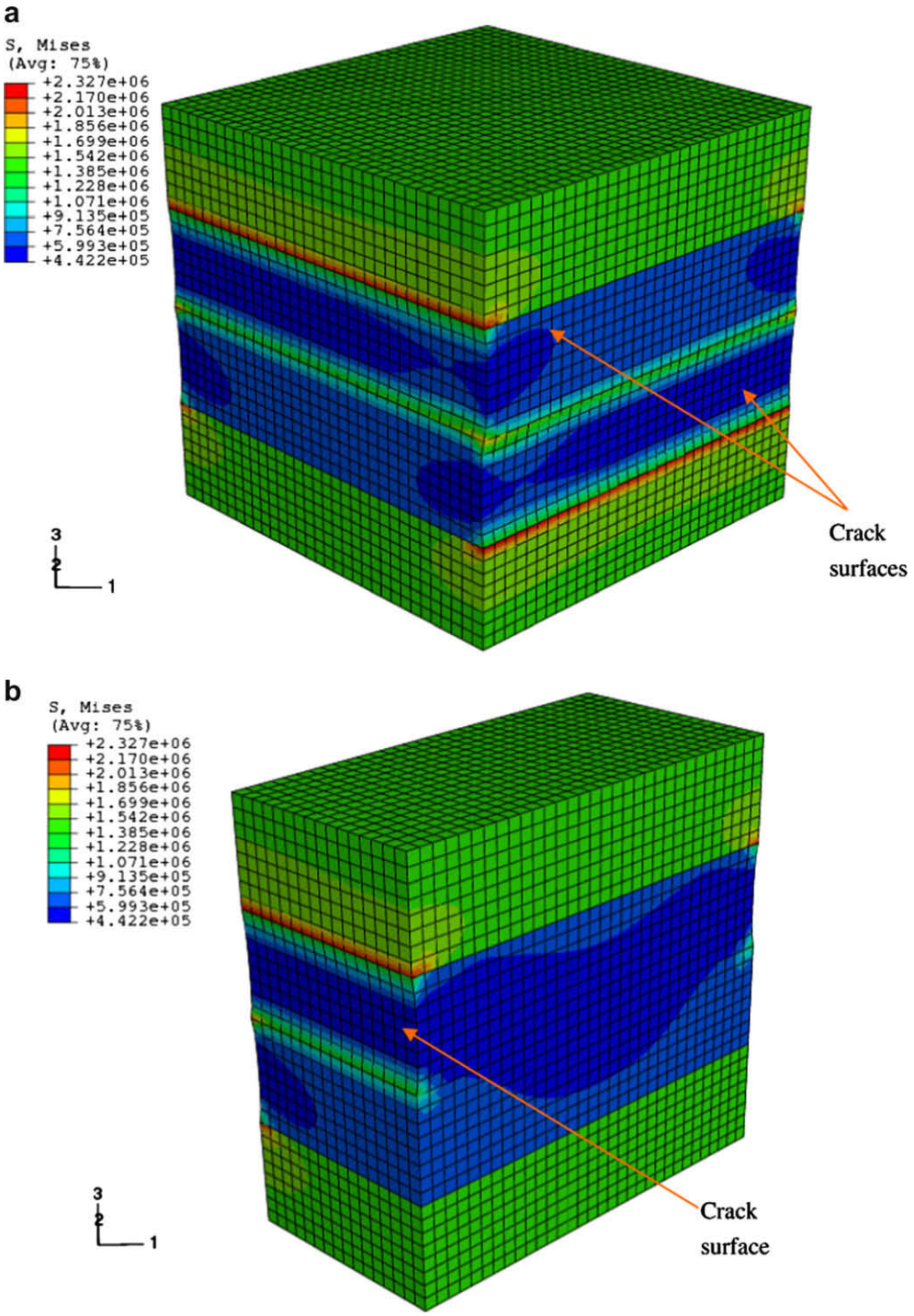

Fig. 4. (a) Stress contour plot at a deformed state of the RVE with applied stress σ_x = 1 MPa. The stresses are shown in Pa (N/m^2). (b) Stress contour plot at a deformed state for half of the RVE with applied stress σ_x = 1 MPa. The stresses are shown in Pa (N/m^2).

For use in 3D analysis, all plies are considered to be transversely isotropic, and hence the thickness direction (index 3) related properties are taken as

$$E_3 = E_2 = 12.7\ \text{GPa};\quad G_{13} = G_{12} = 5.8\ \text{GPa};\quad \nu_{13} = \nu_{12} = 0.297;$$
$$\nu_{23} = 0.42\quad \text{and}\quad G_{23} = E_3/2(1+\nu_{23}) = 4.885\ \text{GPa}$$

FE analysis is performed using ABAQUS® version 6.6. 3D continuum elements (C3D8) are used in FE model. The laminates to be analyzed below are all loaded uniaxially in the x-direction, except in Example 6.3 where uniaxial tension in y-direction and pure shear in the x–y-plane are also applied separately in order evaluate E_y and G_{xy}, respectively. The actual layups vary from one case to another and hence the angles θ_1 and θ_2.

6.1. $[0/\pm45/0]_s$ Laminate with equally spaced cracks in both ±45° plies under axial tension

In relation to Fig. 3, the laminate under consideration corresponds to a case with $\theta_1 = 45°$ and $\theta_2 = -45°$. The crack spacing in both cracked plies is both assumed to be 1 mm. Following Li and Wongsto (2004), a concentrated 'force' (with a dimension of force times length) of $\sigma_x^0 \times$ volume of the RVE $= 10^{-3}$ MPa $\times$ m^3 is applied to the extra degree of freedom ε_x^0. Effectively, this will result in a macroscopically uniaxial stress $\sigma_x^0 = 1$ MPa. The magnitude of the load applied affects the magnitudes of the macroscopic strains obtained. However, the effective properties of the laminated obtained will be fully independent of it.

The extra or key degrees of freedom associated with macroscopic strains as introduced in Li (1999, 2001) and Li and Wongsto (2004) represent a unique feature unavailable in unit cells or RVE as found from other sources in the literature. They offer huge conveniences in applying loads, evaluating average stresses and strains in the unit cell or RVE and calculating the effective properties of the material represented by the unit cell. In the actual FE analyses, they can be introduced by defining several additional nodes which node numbers not occupied by other physical nodes in the mesh. They can be located anywhere and, without losing generality, they can be put at the origin of the coordinate system for the mesh. The degrees of freedom at these nodes are not associated with any particular directions as conventional degrees of freedom. However, they can be treated in the FE analysis in the same way as conventional degrees of freedom in the sense that a concentrated force can be applied to any of them as the 'load' as required or, if a value is imposed to any of them as prescribed 'nodal displacement' as a boundary condition, a reaction can be expected at this degree of freedom. Any of them can, of course, be left free, i.e. no imposed 'nodal displacement' as a boundary condition or 'concentrated force' as a load, in which case, a 'nodal displacement' will be expected at the degree of freedom as a result of deformation. The only difference is that the 'nodal displacement' obtained at any of these extra or key degrees of freedom gives a macroscopic strain directly instead of physical displacement or rotation in any particular direction as of a conventional degree of freedom.

Out of the ABAQUS® analysis, the macroscopic strains obtained at those extra degrees of freedom as the 'nodal displacements' are found as

$$\varepsilon_x^0 = 33.499\times10^{-6},\quad \varepsilon_y^0 = -14.380\times10^{-6}\quad \text{and}\quad \gamma_{xy}^0 = 1.1843\times10^{-9}$$

Apparently, the shear component is nothing but numerical rounding error as it is several orders of magnitude lower than the other strains. From these macroscopic strain values and applied macroscopic stress, the effective properties of the cracked laminate can be obtained as

$$E_x = 29.852\ \text{GPa},\quad \nu_{xy} = 0.4293$$

as opposed to those in the virgin laminate

$$E_x^0 = 31.097\ \text{GPa},\quad \nu_{xy}^0 = 0.4149$$

They represent a 4% and 3.5% change in the effective Young's modulus and Poisson's ratio of the laminate, respectively, due to the presence of transverse cracks in the ±45° plies of the laminate. The increase in the Poisson's ratio results from reduced in-plane shear stiffness (hence, increased shear strain) along the fibers (in 45° to the x-axis) in each ply due to the presence of cracks. This can be demonstrated using a laminate theory if one reduces the in-plane shear modulus along fibers artificially.

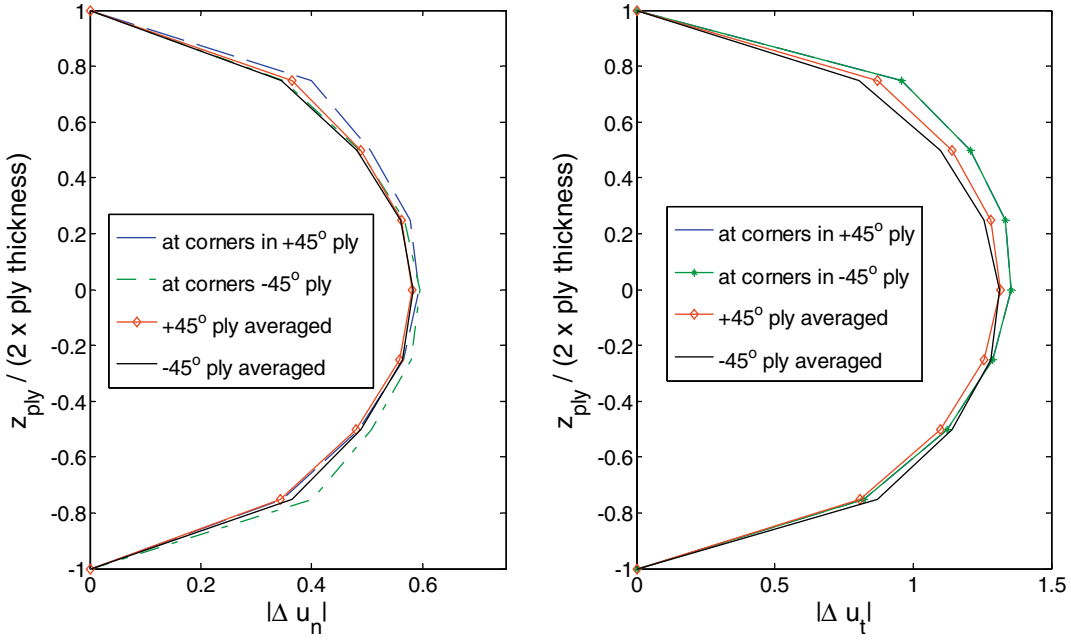

Fig. 5. Distributions of relative normalized displacements between opposite crack surfaces over the thickness of cracked plies.

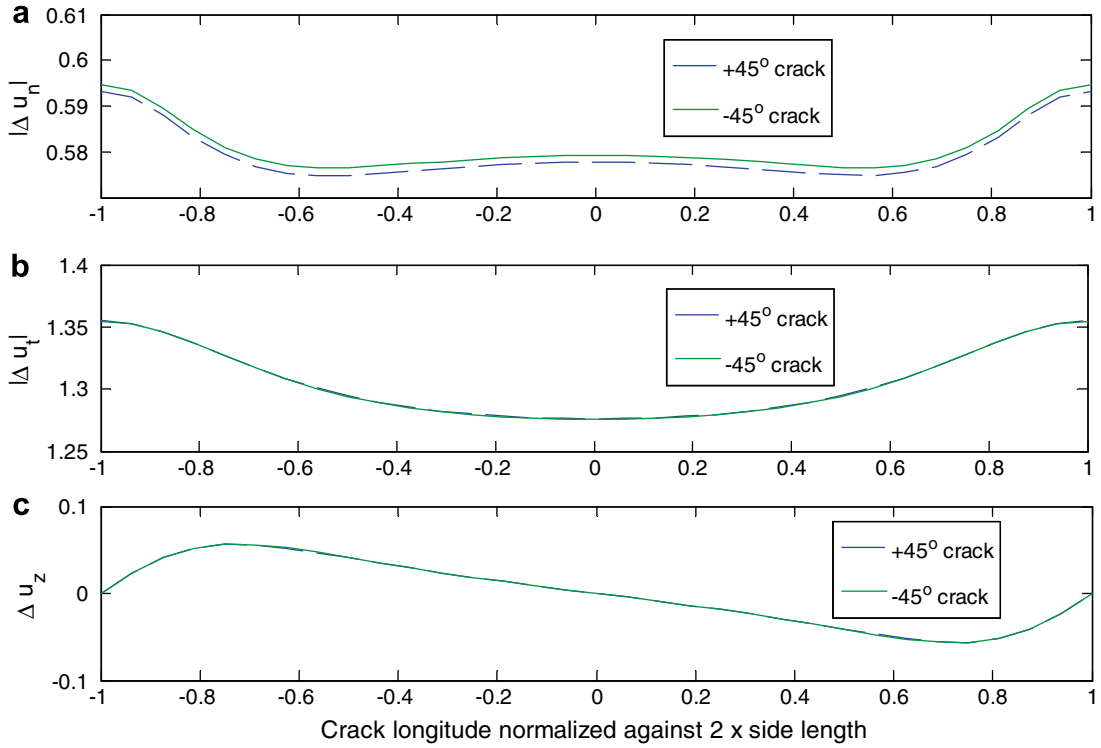

Fig. 6. Distributions of relative normalized displacement between opposite crack surfaces along the side of the RVE. The graphs of $|\Delta u_t|$ and Δu_z are indistinguishable for +45° and −45° layers.

The deformed state of the RVE (with a deformation magnification factor of 3000) is presented in Fig. 4(a) with the mesh shown which is regular all over. The contours are for Mises stress, which may not be particularly meaningful for composites in general. However, as an indication of the stress distribution, they are perhaps informative enough for the present purpose of discussion. Highest stress concentrations are found on the interfaces between the 0° plies and the ±45° plies where the crack edges are located. The next region of stress concentration is between the ±45° plies where mutual constraining effects are the strongest and, therefore, there is less straining than at other interfaces. Away from crack edges, uniform stress distribution resumes, as expected, e.g. between the 0° ply at the bottom and the +45° ply above it. Readers are reminded that stress levels as indicated in the legend is in response to 1×10^6 (Pa) of average stress in uniaxial tension as applied load. The deformation of the crack surfaces is a combination of opening and in-plane shearing modes, which will be described quantitatively later. For more insight into the RVE, a half of the RVE is shown in Fig. 4(b), where the depth of crack affected zones can be seen clearly. In the middle of the RVE, stress distribution is perfectly uniform across the ±45° interface. This is expected to change as the crack density increases.

The opening (normal the crack) and sliding (tangential to the crack) displacements of the cracked surfaces are important parameters in the damage analysis of cracked laminates. A larger opening of cracks suggests more severe degradation in the stiffness properties of the laminate. The synergistic damage mechanics (SDM) approach suggested by Singh and Talreja (2008, submitted to for publication) utilizes this fact to characterize damage effects in multidirectional laminates. The average crack opening displacement, in a general sense, may depend upon laminate material, its layup and the ply thicknesses. The present computational approach provides an appropriate way of obtaining the crack surface displacements.

For the present laminate system, the distributions of relative normalized displacements between opposite crack surfaces normal and tangential to the crack surface, Δu_n and Δu_t, respectively, along the edges at corners of the RVE are plotted in Fig. 5. The displacements are normalized with respect to ply thickness and opening and macroscopic strain, i.e.

$$\Delta u_n = \frac{u_n^+ - u_n^-}{t_c \varepsilon_x^0}, \quad \Delta u_t = \frac{u_t^+ - u_t^-}{t_c \varepsilon_x^0} \tag{17}$$

where the superscripts + and − denote two opposite crack surfaces, t_c is the cracked ply thickness, and ε_x^0 is the macroscopic strain in axial direction. In the figure, the absolute values are shown for the ease of comparisons as their signs may change from one face to another. Although both displacements share a similar profile, the magnitudes are rather different. Given the ±45° ply angles of the cracked plies, it is expected that significant sliding due to in-plane shear would arise. It is in fact more than twice the opening displacement normal to the crack surface. Across the width of the RVE, there is little variation in these distributions. The locations of most difference are at the corners of the RVE. Even there, the comparison with the average does not suggest anything significant.

Along the mid-planes of the cracked plies, the relative normalized displacements between opposite crack surfaces have been plotted along the side of the RVE in Fig. 6. The displacements normal to the crack surfaces, termed as the crack opening displacements (COD), and denoted by $|\Delta u_n|$, are plotted against normalized crack longitude in Fig. 6(a). The different lines show the averaged values normalized with respect to half width of the cracked +45° and −45° plies. The corresponding plots for displacements tangential to the crack surfaces, termed as the crack sliding displacements (CSD), and denoted by $|\Delta u_t|$, are shown in Fig. 6(b). In the figures, dotted blue[2] lines represent +45° ply, whereas solid

[2] For interpretation of the references to color in Fig. 6, the reader is referred to the web version of this paper.

Table 1
Comparison between FE results and experimental data (Varna et al., 1999) for cracked $[0/\pm\theta_4/0_{1/2}]_s$ laminate.

θ (°)	Macroscopic strains at extra degrees of freedom			Effective properties					
				Undamaged laminate		Damaged laminate			
	ε_x^0	ε_y^0	γ_{xy}^0	E_x^0	ν_{xy}^0	E_x/E_x^0		ν_{xy}/ν_{xy}^0	
						FEM	Experiment	FEM	Experiment
55	67.223 μ	−23.275 μ	0.124 μ	18.99 GPa	0.3435	0.78	0.71	1.01	1.04
70	85.737 μ	−12.111 μ	0.356 μ	17.88 GPa	0.18	0.65	0.63	0.79	0.69

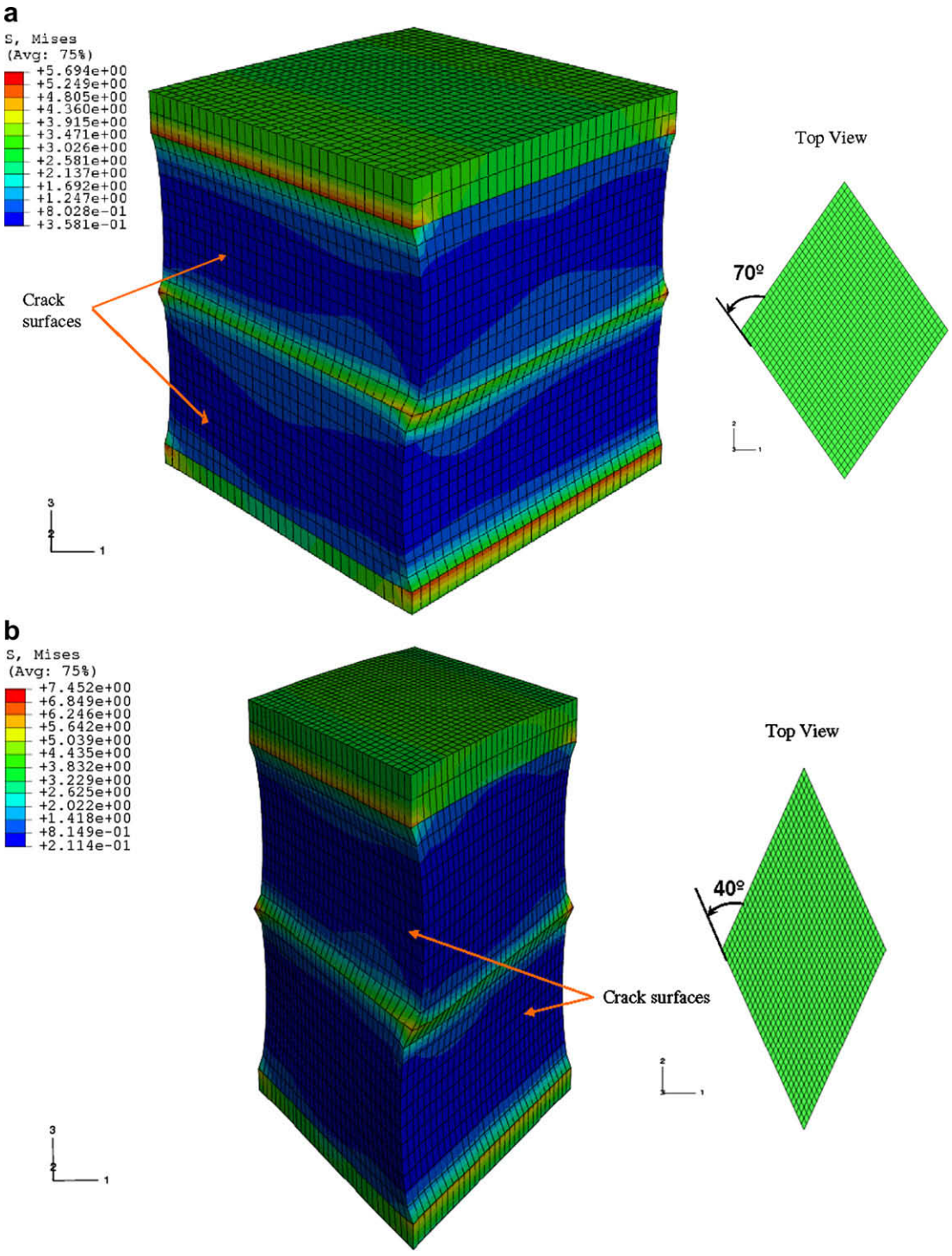

Fig. 7. (a) Stress contour plot at a deformed state of the RVE for cracked $[0°/\pm55_4/0°_{1/2}]_s$ laminate with applied stress $\sigma_x = 1$ MPa. The stresses are shown in MPa. (b) Stress contour plot at a deformed state of the RVE for cracked $[0°/\pm70_4/0°_{1/2}]_s$ laminate with applied stress $\sigma_x = 1$ MPa. The stresses are shown in MPa.

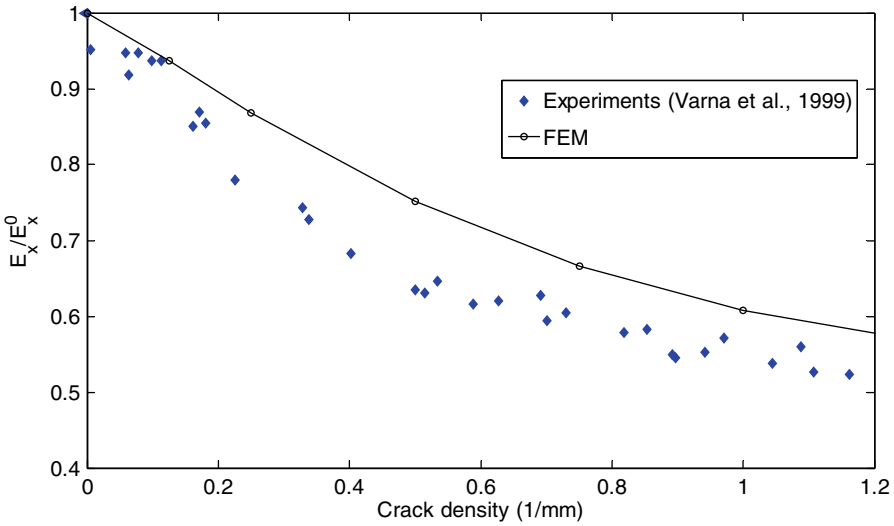

Fig. 8. Comparison of FE simulations with experiments for longitudinal Young's modulus, $\theta = 70°$.

green lines represent $-45°$ ply. The difference in $|\Delta u_t|$ between the $+45°$ and $-45°$ plies is observed to be insignificant at all points along the crack longitude, while the difference in $|\Delta u_n|$ is small, but almost constant throughout the crack longitude. This implies that there is almost the same constraint on both of the $+45°$ and $-45°$ plies from the supporting $0°$ plies. The variations across the width of the RVE are almost negligible, noticing the small scales adopted in this figure. However, the trend of variations agrees well with what is expected. The constraint to the cracks from a neighbouring ply with fibers at $90°$ to the crack surface is hardly weakened by the presence of cracks in the constraining ply. This explains the reason for lack of variation in the distributions in Fig. 6. Should the cracks in the constraining ply make any difference, it is to weaken the constraint at the location of the cracks (i.e. both ends in Fig. 6) and hence increased crack surface displacements are found there. The relative displacement in the thickness direction Δu_z is an order of magnitude smaller than the rest, as shown in Fig. 6(c). Although it is insignificant in magnitude, the pattern of variation conforms with common sense as it suggests a local twisting effect due to the fact that $+45°$ and $-45°$ plies are not in the same plane. However, this twisting effect has been largely suppressed globally as a laminate because of the symmetric layup. The overall average crack surface displacements, in opening and in-plane shearing modes, respectively, are found (scaled to correspond to a 0.5% macroscopic strain level) as

$$\langle \Delta u_n \rangle = 0.53\ \mu\text{m} \quad \text{and} \quad \langle \Delta u_t \rangle = 1.22\ \mu\text{m}$$

as taken from the one of the cracked plies while the same from the other are expected to be literally identical.

6.2. $[0/\pm\theta_4/0_{1/2}]_s$ Laminate with equal crack spacing in both $\pm\theta_4$ plies under axial tension

To enable comparison with the experimental data, the crack spacing in the cracked plies is assumed equal to 1.25 mm. The stress analysis is performed for $\theta = 55°$ and $70°$. Similar to the previous analysis, a concentrated force corresponding to a macroscopic, axial stress of 1.0 MPa in the x-direction is applied on the RVE through the extra degree of freedom ε_x^0. The magnitude of the concentrated 'force' is equal to $\sigma_x^0 \times$ volume of the RVE.

For $\theta = 55°$ laminate: the magnitude of the concentrated force = 1.7435703×10^{-3} MPa $\times$ m^3.

For $\theta = 70°$ laminate: the magnitude of the concentrated force = 1.1926723×10^{-3} MPa $\times$ m^3.

The macroscopic strains as obtained from the FE analysis as the nodal displacements at the extra degrees of freedom are shown in Table 1. Also included in the table are the effective properties of the cracked laminates derived from the applied macroscopic stress and the obtained macroscopic strains.

In the experimental work, Varna et al. (1999) evaluated the effect of cracking in $[0/\pm\theta_4/0_{1/2}]_s$ laminates subjected to tensile loading in axial direction. The laminate specimens were observed to have nearly same crack density in $+\theta$ and $-\theta$ layers at a given loading. The full-size specimens (20 mm width) were loaded in an Instron 1272 testing machine to measure residual elastic properties at different states of damage and to characterize damage (density of cracks in the $\pm\theta$-plies) in the laminates at increasing tensile loads. Thin strips (3.5 mm width) were then cut longitudinally from the cracked specimens and were placed in a set-up developed for measuring COD. The set-up consisted of a miniature materials tester (MINIMAT) for loading the thin strip to open cracks, which were observed by an optical microscope equipped with a video camera. The micro-specimens (thin strips) were loaded at two pre-selected longitudinal strains, for the COD measurements. A specially constructed mini-extensometer was used to measure strains on the micro-specimens. These strains were much below the strains in the macro-specimens at which the intralaminar cracks were produced, thus generating no further cracking.

The FE predictions are compared with the experimental data in Table 1 at a crack spacing equal to 1.25 mm. In general, the FE results compare well with the experimental data. However, for $\theta = 55°$, it is important to note that the experimental data showed shear induced damage which has not been considered in the FE analysis performed above. For $\theta = 70°$, FE results show less reduction in the Poisson's ratio than that observed in experiments but the experimental data showed a large scatter in the Poisson's ratio (Varna et al., 1999).

The contours for the Mises stress are shown in Figs. 7(a) and (b) on the deformed configuration of the RVE with a deformation magnification factor of 1000 for $\theta = 55°$ and $70°$, respectively. Top views of the two meshes of the RVEs for these laminates are shown as insets in these figures. They are both skewed, as expected. It should be noted that the mesh is not fine enough to give reasonable stress

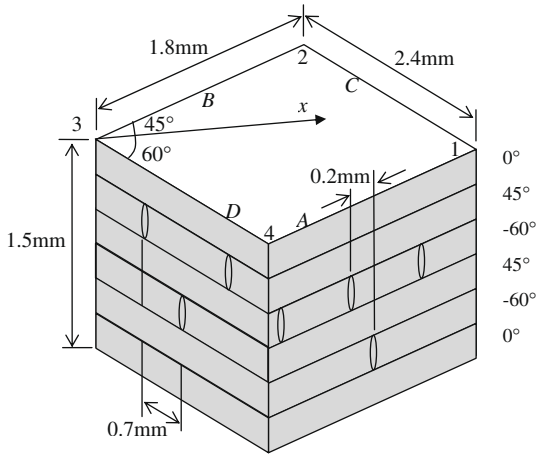

Fig. 9. RVE of Example 6.3.

and displacement contours near the crack tips for practical considerations. The presented results are for illustration primarily.

In the particular case of $[0°/\pm 70_4/0°_{1/2}]_s$ laminate, experimental data were available (Varna et al., 1999) for the stiffness reduction as crack density increases. FE predictions have been made correspondingly and compare with experimental data in Fig. 8. The agreement is good, bearing in mind that the FE mesh is fairly coarse which tends to provide a stiffer response.

6.3. $[0/-60/45/-60/45/0]_s$ Laminate with unequal crack spacing in $-60°$ and $45°$ plies under combined tension and shear

This is a case to illustrate the wide range the proposed RVE construction is capable of covering. The crack spacing in the upper $-60°$ ply is different and 3 times that in the other $-60°$ ply. The locations of the cracks in these two plies are staggered with an offset as shown in Fig. 9. The crack spacings in the two $45°$ plies are unequal as well, and one is twice the other. The locations of the cracks in these two plies are also staggered as shown in Fig. 9. The RVE is depicted in Fig. 10. The macroscopic stress ratio is assumed to be at $\sigma_x^0 : \sigma_y^0 : \tau_{xy}^0 = 2 : 1 : 1$ (with $\sigma_x^0 = 1.0$ MPa).

With the current laminate configuration loaded in axial tension, there will be cracks in all but the $0°$ plies within the RVE. It makes sense to avoid cracks on the surfaces so that boundary conditions can be applied slightly easier, as suggested in Fig. 2(b).

The macroscopic strains obtained at the extra degrees of freedom are

$$\varepsilon_x^0 = 31.162 \times 10^{-6}, \quad \varepsilon_y^0 = 13.952 \times 10^{-6} \quad \text{and} \quad \gamma_{xy}^0 = 48.788 \times 10^{-6}$$

Here, the shear strain is quite high due to the loading condition and laminate layup. There is no data available to validate the analysis. Rather, the case could serve as a benchmark case for future studies to demonstrate the capability of the RVE proposed.

The contours for the Mises stress in the RVE under combined shear and tensile loading condition ($\sigma_x = 1$ MPa; $\sigma_y = \tau_{xy} = 0.5$ MPa) with a deformation magnification factor of 3000 are shown in Fig. 10. The mesh adopted is not fine enough to capture all the details in stress distribution, which was not the purpose of the present exercise. However, at the present level of resolution, it is possible to observe that the cracks in the $-60°$ plies are subjected to more crack opening displacement than those in the $45°$ plies. This is due to the applied loading case and the laminate layup. A simple laminate analysis of the same laminate without cracks suggests higher laminar stress in the direction transverse to the fibers (hence to the cracks) in the $-60°$ plies than that in the $45°$ plies. Thus, more crack opening displacement is expected in the $-60°$

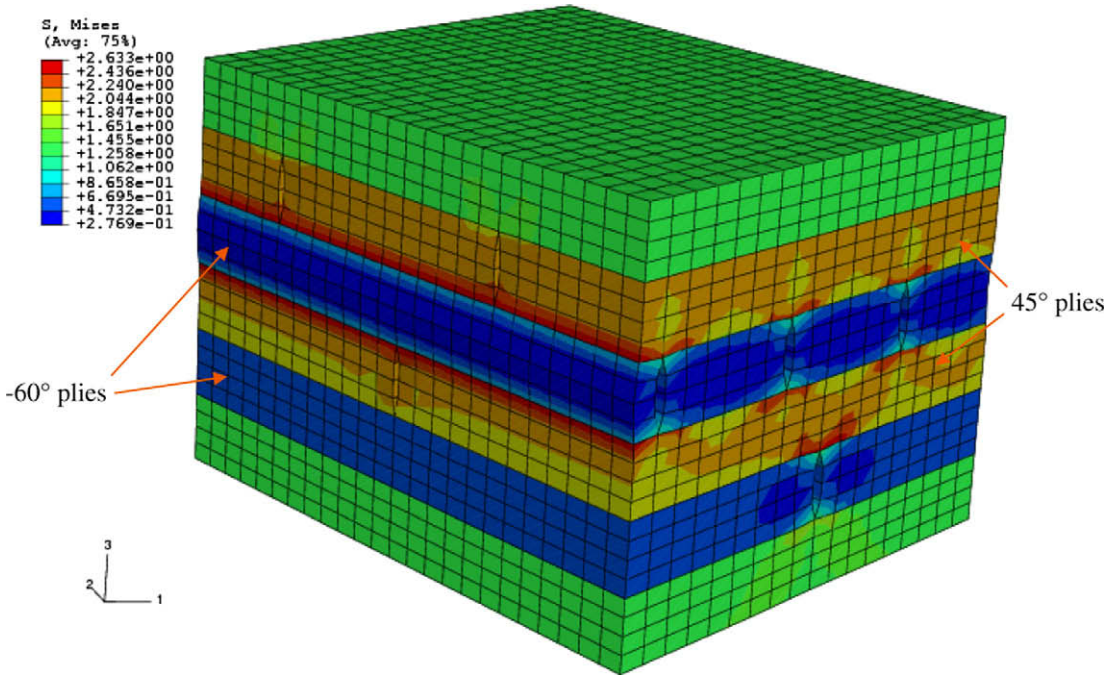

Fig. 10. Stress contour plot at a deformed state of the RVE for cracked $[0/-60/45/-60/45/0]_s$ laminate with applied stress $\sigma_x = 1$ MPa, $\sigma_y = \tau_{xy} = 0.5$ MPa. The stresses are shown in MPa.

Table 2
Macroscopic strains and effective properties for cracked $[0/-60/45/-60/45/0]_s$ laminate.

Loading case	Macroscopic strains at extra degrees of freedom			Effective properties
	ε_x^0	ε_y^0	γ_{xy}^0	
Virgin material	–	–	–	$E_x^0 = 25.31$ GPa; $E_y^0 = 20.38$ GPa; $G_{xy}^0 = 9.87$ GPa; $v_{xy}^0 = 0.3510$; $v_{yx}^0 = 0.2827$
$\sigma_x = 1$ MPa; $\sigma_y = \tau_{xy} = 0$	42.340 μ	−15.081 μ	−7.275 μ	$E_x = 23.62$ GPa; $v_{xy} = 0.3562$
$\sigma_y = 1$ MPa; $\sigma_x = \tau_{xy} = 0$	−15.081 μ	51.694 μ	6.371 μ	$E_y = 19.35$ GPa; $v_{yx} = 0.2917$
$\tau_{xy} = 1$ MPa; $\sigma_x = \tau_y = 0$	−7.27 μ	6.371 μ	105.750 μ	$G_{xy} = 9.46$ GPa

plies. As a result, more stress concentrations as indicated by the stress contours are seen at the crack edges in these plies than in the 45° plies.

It can also be observed from the deformation pattern shown in Fig. 10 that the sides of the RVE do not remain plane after deformation. They would, if the reflectional symmetry conditions had been used instead of translational ones. However, the laminate layup and the damage pattern do not possess such reflectional symmetries. In other words, any attempt to impose boundary conditions such that the sides remain plane after deformation would lead to incorrect results, as there is no reason in the present case to justify such boundary conditions.

The same RVE can be analyzed for other loading cases under macroscopically uniaxial direct stress or shear stress in order to evaluate the effective properties of the cracked laminate. The macroscopic strains and the corresponding effective properties derived from the results of these loading cases are presented in Table 2.

From the effective properties shown in Table 2, the lack of orthotropy is obvious, as given by the presence of the macroscopic shear strains under macroscopic direct stresses. However, the symmetry of the effective stiffness matrix (as a condition for the existence of strain energy density) of the cracked laminate is preserved, as validated by the reciprocal relation, $v_{yx} = v_{xy}\frac{E_y}{E_x} = 0.3562\frac{19.35}{23.62} = 0.2917$.

7. Conclusions

By considering the translational symmetries present in cracked laminates with two independent arrays of cracks in different directions, not necessarily orthogonal, an RVE can be constructed with boundary conditions derived from the symmetry conditions without compromising their precision. The approach is systematic and straightforward to apply. The use of the proposed RVE has been demonstrated through three different examples illustrating the wide range of its applicability. While the validity of the present formulation relies on its mathematical rigor, the favorable comparisons against experimental data give confidence in the use of the RVE in analysis of cracked laminates. The results obtained here for unequal cracking in two different directions, with staggered placement of cracks in the plies, may not be possible without the use of the proposed RVE construction. It can be claimed that the work presented in this paper has extended the existing capability for analyzing laminates with two cracking systems subjected to the geometric restriction of the proposed RVE.

Acknowledgments

The first author is indebted to Professor Ramesh Talreja and the Department of Aerospace Engineering of Texas A&M University for offering him the financial support during his stay at the Department where the work in this paper was conducted. He also wishes to thank The Royal Academy of Engineering, UK for providing him with an International Travel Grant (IJB/PS/J7-986).

References

Garrett, K.W., Bailey, J.E., 1977. Effect of resin failure strain on tensile properties of glass fiber-reinforced polyester cross-ply laminates. J. Mater. Sci. 12 (11), 2189–2194.
Grufman, C., Ellyin, F., 2007. Determining a representative volume element capturing the morphology of fiber reinforced polymer composites. Compos. Sci. Technol. 67 (3–4), 766–775.
Hashin, Z., 1985. Analysis of cracked laminates: a variational approach. Mech. Mater. 4 (2), 121–136.
Hashin, Z., 1987. Analysis of orthogonally cracked laminates under tension. J. Appl. Mech. Trans. ASME 54 (4), 872–879.
Jin, K.K., Huang, Y., Lee, Y.H., Ha, S.K., 2008. Distribution of micro-stresses and interfacial tractions in unidirectional composites. J. Compos. Mater. 42 (18), 1825–1849.
Li, S., 1999. On the unit cell for micromechanical analysis of fiber-reinforced composites. Proc. Roy. Soc. Lond. A 455 (1983), 815–838.
Li, S., 2001. General unit cells for micromechanical analyses of unidirectional composites. Composites A 32 (6), 815–826.
Li, S., 2008. Boundary conditions for unit cells from periodic microstructures and their implications. Compos. Sci. Technol. 68 (9), 1962–1974.
Li, S., Wongsto, A., 2004. Unit cells for micromechanical analyses of particle-reinforced composites. Mech. Mater. 36 (7), 543–572.
Li, S., Reid, S.R., Soden, P.D., 1994. A finite strip analysis of cracked laminates. Mech. Mater. 18 (4), 289–311.
McCartney, L.N., 1992. Theory of stress transfer in a 0-degrees-90-degrees-0-degrees cross-ply laminate containing a parallel array of transverse cracks. J. Mech. Phys. Solids 40 (1), 27–68.
Noh, J., Whitcomb, J., 2001. Effect of various parameters on the effective properties of a cracked ply. J. Compos. Mater. 35, 689–712.
Singh, C.V., Talreja, R., 2008. Analysis of multiple off-axis ply cracks in composite laminates. Int. J. Solids Struct. 45 (16), 4574–4589.
Singh, C.V., Talreja, R., submitted to for publication. A synergistic damage mechanics approach for composite laminates with matrix cracks in multiple orientations, Mech. Mater.
Varna, J., Berglund, L., 1991. Multiple transverse cracking and stiffness reduction in cross-ply laminates. J. Compos. Tech. & Research 13 (2), 97–106.
Varna, J., Joffe, R., Akshantala, N.V., Talreja, R., 1999. Damage in composite laminates with off-axis plies. Compos. Sci. Technol. 59 (14), 2139–2147.
Xia, Z., Zhang, Y., Ellyin, F., 2003. A unified periodical boundary conditions for representative volume elements of composites and applications. Int. J. Solids Struct. 40 (8), 1907–1921.
Xia, Z., Zhou, C., Yong, Q., Wang, X., 2006. On selection of repeated unit cell model and application of unified periodic boundary conditions in micro-mechanical analysis of composites. Int. J. Solids Struct. 43 (2), 266–278.